# Experimental study and mathematical modeling of the long-term behaviour of sandstone

Xiaoming Sun [a,b,c], Ziyang Feng [a,b,c], Chengyu Miao [d*], Biao Zhang [a,b,c*], Yong Zhang [a,b,c], Zhibiao Guo [a,b,c]

a. Inner Mongolia Research Institute, China University of Mining and Technology (Beijing), Ordos 017000, China

b. State Key Laboratory for Tunnel Engineering, China University of Mining and Technology (Beijing), Beijing 100083, China

c. Key Laboratory of Disaster Prevention and Disposal in Coal Mining, Ministry of Emergency Management, Beijing 100083, China

d. School of Engineering and Technology, China University of Geosciences, Beijing 100083, China

* Corresponding Author:

mcycumtb@163.com (Chengyu Miao)

zhangbiao@bwu.edu.cn (Biao Zhang)

**Abstract:** The short-time compression test and creep test of sandstones with different water content are carried out by using the five- linked rheological experiment system. Based on the experimental results, the effects of confining pressure and different water content on the short-term mechanical behavior of sandstone are analyzed. The results show that the peak strength of sandstone decreases exponentially with water content and increases with confining pressure, and the degree of water weakening of sandstone decreases with the increase of confining pressure. The results of creep test show that during the instantaneous phase the deformation increases with the increase of water content. And the steady creep rate and the ratio of creep stress to compressive strength($\sigma/\sigma_c$) of sandstones with different water content show a uniform exponential increase law under high confining pressure. According to creep stress level, the isochronous curves can be divided into three stages, namely viscoelastic deformation stage, plastic deformation stage, and nonlinear plastic deformation stage. It is found that the two critical stresses which are yield limit strength (i.e. long-term strength) and accelerated yield limit strength, and the compressive strength of sandstones under different water content are in a stable range. Based on the Nishihara model, the creep equation related to creep stress is established and the creep parameters ($E_{c0}$, $E_{c1}$, $\eta_{c1}$) related to initial water content and initial creep stress are obtained, which decreased linearly with water content. Based on the creep rate, a damage factor that can describe the accelerated creep behavior is introduced, and the creep model and constitutive equation of the whole creep process are established. The creep deformation behavior of sandstone under different stress conditions is predicted, and a good fitting effect is acquired. According to the equation, the creep deformation law of sandstone under different creep stress and water content conditions can be described.

***Keywords*:** Creep behaviour; Sandstone; Water-rock coupling; Isochronous curve; Mathematical modeling

## 1 introduction

Coal is China's basic energy and occupies a dominant position in the primary energy structure. At present, mineral resources are developing to deep mining, facing many complicated geological problems unique to deep mining. It includes the nonlinear deformation and failure problems, such as cap and sag, shrinkage and floor heave, caused by high ground stress, high ground temperature, high osmotic pressure and strong mining disturbance. Consider the soft rock strata in Wanfu Coal mine, Shandong Province, China. The adsorption of groundwater causes the surrounding rock strength to soften and fail, and the rock exhibits obvious large deformation characteristics. According to the rock strength softening theory, water will reduce rock strength to varying degrees, which is manifested in the influence on the uniaxial and triaxial compressive strength of rock. The softening degree varies according to the different strength of rock micro-clay mineral content (Wong et al., 2015). The content of clay minerals in sandstone is large, therefore the strength is greatly affected by groundwater. Scholars have studied the influence of different confining pressures on strength, and the mechanical properties of rock will increase with the increase of confining pressures (Wasantha and Ranjith, 2014). The existence of confining pressure limits the lateral deformation of rock and also significantly affects the strength softening degree of rock by water (Li et al., 2012; Rajabzadeh et al., 2012; Zhang et al., 2014). Some scholars have provided the quantitative relationship between them. In general, the strength softening of different rocks shows a negative exponential decline relationship (Miao et al., 2021). On the other hand, scholars have studied the influence of different water content on the long-term strength of rocks (Tang et al., 2018; Yu et al., 2019). Chen et al. (2021) further studied the strength and long-term failure model of sandstones with different water absorption heights through indoor uniaxial creep experiment. Deng et al. (2016) studied the long-term strength and creep failure rule of red-bed sandstone under the action of water-rock circulation through indoor triaxial creep experiment.

Experiments show that when the creep failure of rock specimen occurs, their axial strain creep curves with time all show typical three-stage deformation (Lin et al., 2009; Wang et al., 2021; Zhou et al., 2021). It is generally considered that the critical stress in the initial creep stage and the steady creep stage is the creep limit stress or long-term strength (Cui and Fu, 2006; Cong and Hu, 2017). Creep failure occurs when the strength exceeds this strength for a long enough time. Therefore, in the process of creep model research, the three-parameter (H-K) model was developed to burgess model, and Nishihara model was developed considering the existence of long-term strength (Aydan, 2017; Liu, 1994). On this basis, many scholars also conducted in-depth research on the model and established a large number of modified models and new combined models (Jiang et al., 2016; Tao et al., 2005). Of course, the current research on the first two stages of creep is not limited to simple linear superposition of models. The damage of rock materials caused by different factors were considered, and a more realistic theoretical model based on indoor creep experimental analysis were established. For example, Zheng et al. (2015) described the initial creep and steady-state creep deformation of porous rock mass through the modified Burgess model. Lu and Wang (2017) explored the creep characteristics of mudstone under different water temperatures. Some scholars also use fractional mathematical model (Xu and Cui,2020; Zhou et al., 2011) to study the creep process in two stages of rock creep.

For the study of the accelerated creep stage, there are two methods to judge the accelerated creep stage at present. One is to build an accelerated rheological model with strain as the threshold. Jiang et al. (2013) established a strain-triggered nonlinear pot model to improve the Nishihara model. Yang and Xu (2014) established a nonlinear damage mathematical model based on strain to describe creep aging failure behavior. Wang et al. (2021) established a freezing-thawing cycle damage model to modify the Boggs model and describe the complete creep process. The other is to build a time-threshold accelerated rheological model. For example, Shan et al. (2019, 2020) and Yan et al. (2020) modified the traditional burgess and Nishihara models by using nonlinear fractional order functions. Özşen et al. (2014) studied the creep deformation curve of rock salt by directly providing a time-dependent acceleration mathematical model, and mathematically divided the creep process into the sum of three parts. The above models all explore the whole process of the final creep failure. Starting from the mathematical analysis of the final deformation curve, the corresponding theoretical research is carried out. The nonlinear damage caused by different creep loads in the process is not considered, and the model parameters in the process are considered to be uncertain constants.

In order to further study the variation law of model parameters under different creep loads in the model, this paper adopts the method of increasing the application range of experimental creep load and introducing incremental steps to approach the actual stress inflection point and long-term strength of sandstone during the experiment. Through the detailed analysis of the experimental stress-strain curves the ranges of yield strength and accelerated yield strength are obtained, and based on this, a creep mathematical model is established.

## 2 Sandstone samples and experiment studies

### 2.1 Engineering background

The section shape of -950 horizontal substation of Wanfu Coal Mine is straight wall semi-circular arch, with a width of 6.1m and a height of 5.8m. Anchor net cable spraying support is adopted during roadway excavation, and the design of supporting section is shown in Figure 1. Bolt design anchorage force is not less than 130 kN, and anchor cable design anchorage force is not less than 180 kN. The anchor/cable control of surrounding rock deformation mainly depends on its anchoring force, which is converted into hydrostatic pressure (Wang et al., 2011). The calculated equivalent stresses are 12.02 MPa and 4.16 MPa respectively, and the experimental design is based on the stress.

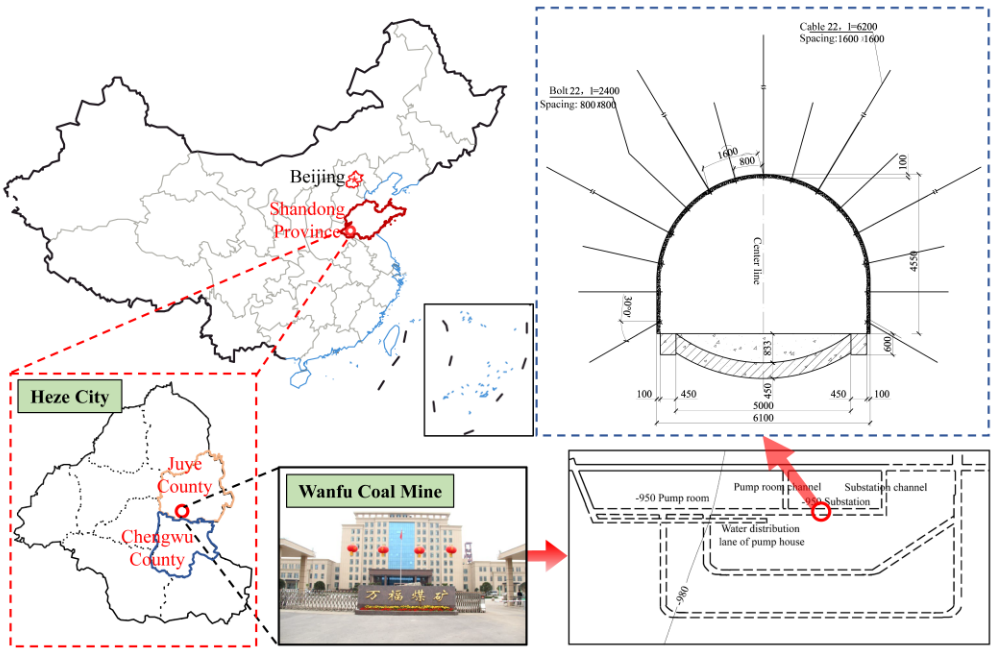


Fig.1. General situation and location of Wanfu Coal Mine.

## 2.2 Sandstone samples

The sandstone samples selected in this paper are taken from the -950 horizontal pump house channel, with a buried depth of about 1040 m. The water content of surrounding rock of the pump house channel ranges from 0.62 to 1.78% after the sandstone samples are retrieved from the site and dried. It is made into a standard cylindrical sample (φ50 mm×100 mm) to ensure the surface smoothness and the parallelism of the upper and lower end faces within the specified error range. Fig. 2 is the XRD experiment results, the sandstone samples are mainly composed of quartz and clay minerals, of which quartz accounts for about 78.5% and clay minerals account for about 17.6%, and also contain a small amount of potash feldspar and olomite. The clay minerals are mainly composed of kaolinite and chlorite, with a small amount of illite and Aemon mixed layer. According to multiple group experimental results, it can be seen that the composition of the samples in this experiment is relatively homogeneous. At the same time, the wave velocity of sandstone samples was measured, and the average wave velocity was 3.52 km/s. Samples with similar wave velocity were selected for experiment to reduce the error between samples.

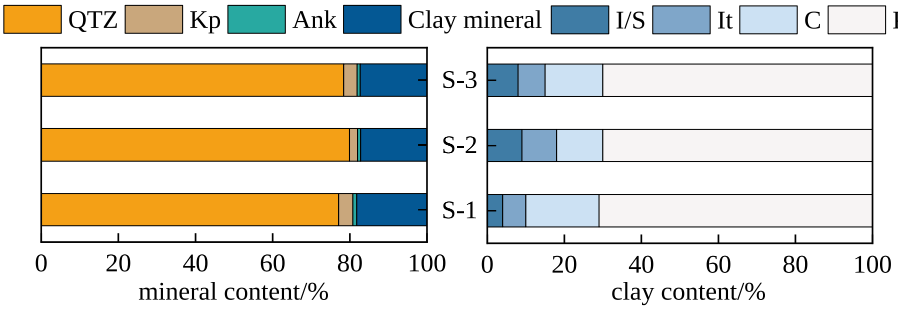


Fig. 2. Mineral composition of sandstone.

### 2.3 Uniaxial and triaxial compression experiment

The saturated water content of sandstone samples was obtained through the initial non-pressure water absorption experiment, and different water content gradients were designed as 0%, 0.8%, 1.6%, 2.4%, and 3.3% (Miao et al., 2021). Fig. 3 shows the five-linked rheological experiment system of State Key Laboratory of Geomechanics and Deep Underground Engineering, China University of Mining and Technology (Beijing). The experimental system provides axial pressure and confining pressure in the triaxial pressure chamber through the pressure controller. After setting the stress required by the creep experiment through the control system, the servo control stage is entered for long-term creep experiment. The system can also conduct short-term strength tests. The compressive strength curves of sandstones with different water content are got through uniaxial and triaxial compression tests, as shown in Fig. 4. It can be found that the rock strength is softened under the influence of water content, while the softening phenomenon decreases when the radial deformation is limited under the influence of confining pressure. The softening coefficient $\eta$ increased greatly from 0.372 to 0.502 under uniaxial condition.

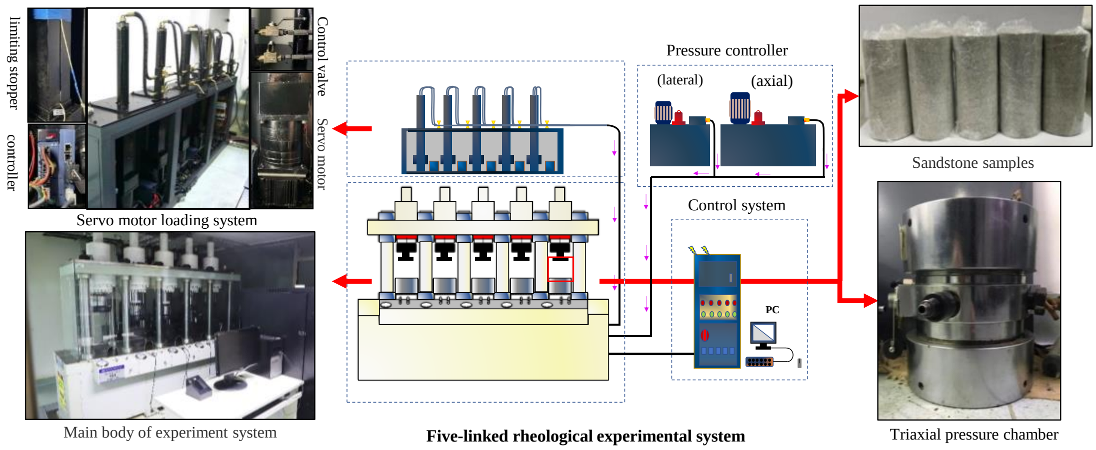


Fig. 3. Experimental system.

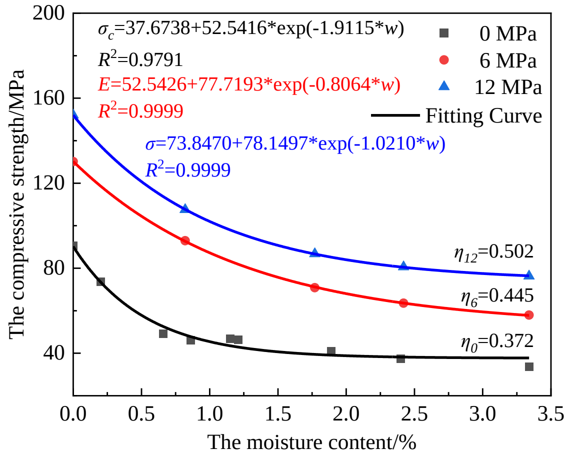


Fig. 4. Experimental curve of sandstone strength softening.

## 2.4 Creep experiment results

There are two main creep loading methods at present, one is single-stage loading and the other is graded loading. In this paper, the single-stage loading method was adopted for the experiment. In order to obtain the deformation and failure curve of the whole creep process, the incremental load was reduced in the late loading stage to avoid the brittle failure of rock. According to the uniaxial test results, the stress level was designed. Considering the low uniaxial compressive strength of saturated samples, the initial creep stress was set as 18 MPa and the stress difference between two adjacent loads was set as 4.5 MPa in order to study the creep response of rock under the same stress state. After the full creep process, the next stage is entered, and the creep time of each stage is designed to be 24 h until the creep failure of the sample occurs. Fig. 5 (a) shows experimental creep curves of five water contents under 12 MPa confining pressure. In terms of experimental data processing, considering that rock creep is nonlinear and does not meet the principle of linear superposition, Chen loading processing method will be used for data processing (Liu, 1994). Meanwhile, the elastic deformation and creep deformation in the creep process can be preliminarily separated by this method, and the specific results are shown in Fig. 5(b, c). It can be found that as the creep stress increases, the instantaneous strain increases and shows a linear increase relationship with the stress. The steady-state creep rate is further processed, and the evolution law of steady creep with the ratio of creep stress to compressive strength ($n_c$) under different moisture content and different creep stress levels was got. It can be found that although the water content of sandstone is different, it has a non-linear increasing relationship with compressive strength $n_c$. The mathematical relationship between them is preliminarily fitted through fitting, as shown in Fig. 6.

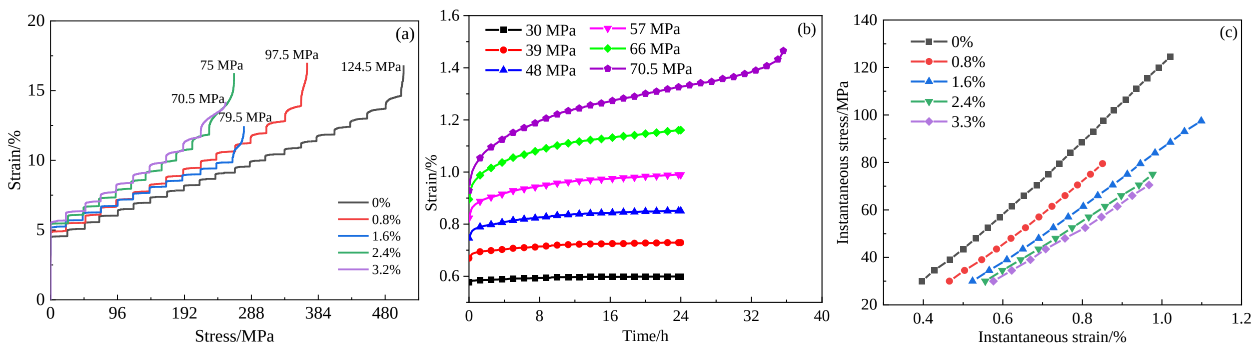


Fig. 5. Creep curves of sandstone with different water content of 12MPa. (a) creep curve. (b) graded creep curve. (c) instantaneous strain.

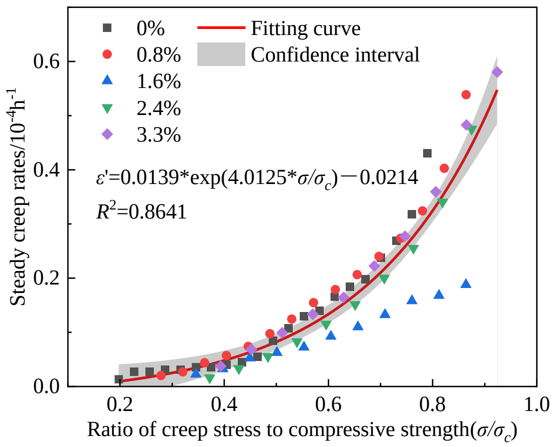


Fig. 6. Triaxial steady creep rate of sandstone under 12MPa confining pressure.

# 3 Experimental studies

## 3.1 Isochronous curve and critical stress

The long-term strength of rock is an important index to measure the long-term stability of rock, and the creep and long-term strength laws are studied by means of graded loading in the indoor process (Lu and Wang, 2017; Sun et al., 2021). Scholars have adopted the isochronous stress method to study the stress inflection point and long-term strength in laboratory experimental data of rocks (Wu et al., 2020; Liu et al., 2020). Theoretically, when the creep load is small enough and the experimental samples are sufficient, the isochronous curve can approach the long-term strength indefinitely. From the current study, it is found that the instantaneous elastic deformation is much larger than the viscoelastic creep deformation. The initial elastic strain of saturated sample is $5.76\times10^{-3}$, while the creep strain is only $2.3\times10^{-4}$. In order to reduce the influence of elastic deformation, the viscoelastic-plastic creep curve was treated isochronously to obtain multiple strain curves at different times. The 3-hour and 24-hour curves are shown in Fig. 7.

It can be found that when the creep stress is small, the final deformation remains unchanged after creep deformation and does not enter the steady creep stage (only viscoelastic deformation). Taking this stage as the first stage, the Kelvin model is often used in previous studies to describe the creep behavior. When the stress is greater than a certain stress, plastic deformation occurs. The creep enters the next stage, and this critical stress is also called the long-term strength. At this stage, although the plastic strain develops slowly, as long as the time is enough, it will enter the final accelerated creep stage and finally produce creep failure. The critical stress is defined as yield stress $\sigma_s$. The viscoplastic model is superimposed on Nishihara model to describe the plastic deformation after the yield stress is exceeded by the stress. Generally, it is considered that different creep stresses produce different creep effects, so the corresponding creep parameters are non-constant. By analyzing the data in Fig. 6, it is found that there is a linear growth relationship between the plastic deformation and creep stress in a stage t of plastic deformation process. . Therefore, this stage is divided into the second stage. When the stress is greater than the critical stress, the nonlinear plastic deformation occurs and the creep enters third stage. The critical stress is defined as the accelerated yield stress $\sigma_{as}$.

The viscoelastic deformation and plastic deformation in different stages are studied. when the stress exceeds the yield stress, it is found that the viscoelastic deformation of the whole line continues to develop steadily on the left side, by extending the final deformation straight line of the first stage upwards. The area enclosed by the upward extension of the line and the viscoelastic deformation line is the plastic deformation with stable development in the second stage. In addition, the amount of deformation exceeding the stable plastic deformation in the third stage is defined as nonlinear deformation. In this classification process, the deformation development at the final accelerated failure stage is not considered.

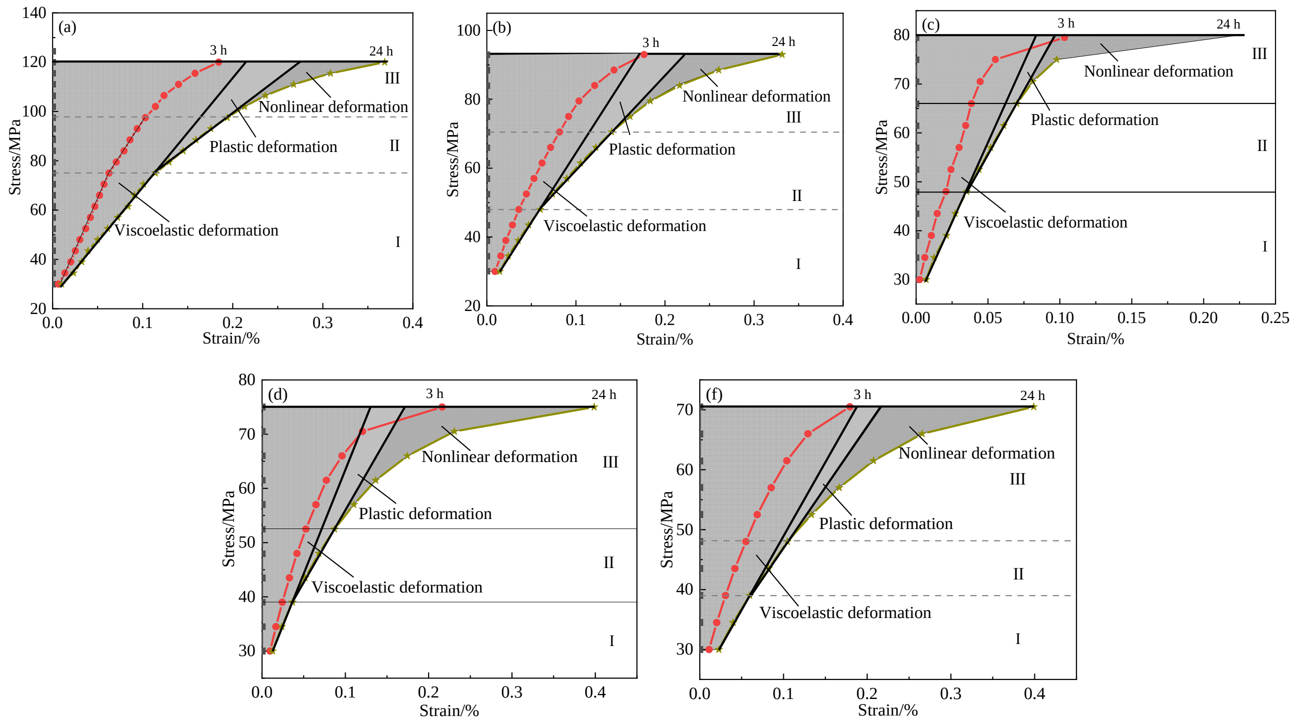


Fig. 7. Deformation separation diagram of creep isochronous curve with confining pressure of 12 MPa. (a) SR-30. (b) SR-31. (c) SR-32. (d) SR-33. (e) SR-34.

Different critical stresses and compressive strengths of sandstones under 12MPa confining pressure are recorded in Table 1. Similar to the compressive strength, the yield limit and accelerated yield limit decrease with the increase of water content. The ratio of critical strength to compressive strength remained within a stable range, in which the ratio of yield stress to compressive strength ($n_s$) was between 0.45 and 0.55, and the ratio of accelerated yield stress to compressive strength ($n_{as}$) was between 0.63-0.71. It can be considered that the ratio of creep stress to compressive strength ($n$) can be used to describe the influence of water content on the mechanical behavior of sandstone under relatively large confining pressure to a certain extent.

Table 1 creep yield limit and accelerated yield limit under 12MPa confining pressure.

| Confining pressure /MPa | Water content /% | 0% | 0.8% | 1.6% | 2.4% | 3.3% |
|---|---|---|---|---|---|---|
| | Compressive strength $\sigma_{12}$/MPa | 152.0 | 107.6 | 86.8 | 80.6 | 76.3 |
| 12 | Yield limit strength $\sigma_s$/MPa | 75 | 48 | 48 | 39 | 39 |
| | $\sigma_s/\sigma_{12}$ ($n_s$) | 0.49 | 0.45 | 0.55 | 0.48 | 0.51 |

| | | | | | |
|---|---|---|---|---|---|
| Accelerated yield limit strength $\sigma_{as}$/MPa | 97.5 | 70.5 | 65 | 52.5 | 48 |
| $\sigma_{as}/\sigma_{12}$ ($n_{as}$) | 0.64 | 0.66 | 0.75 | 0.65 | 0.63 |

3.2 Traditional Nishihara model fitting

According to the definition of the traditional Nishihara model, the Nishihara model can be used to describe the linearly developed part of elastic and viscoelastic-plastic deformation, as shown in Fig. 8. Although in traditional studies, when the stress exceeds the long-term strength, the Nishihara model can be used to describe the creep process, and the parameters are considered to be uncertain constants. From the above studies, it is found that the relationship between plastic deformation and creep stress show a linear increase in the second stage, which can be identified by using the creep Eq. (1) of the Nishihara model (Zhang and Wang, 2020). The parameters should have the same linear relationship, so the statistic creep parameters of the sample with 12 MPa confining pressure are shown in Table 2, and the relationship between parameters and stress of SR-30 sample is drawn as shown in Fig. 9.

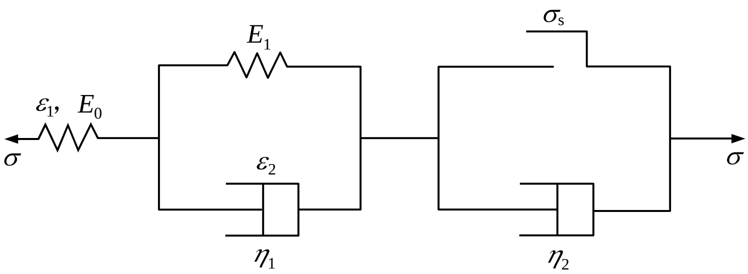


Fig. 8. Nishihara model.

$$\left.\begin{aligned} \varepsilon &= \frac{\sigma_0}{E_0} + \frac{\sigma_0}{E_1}\left(1 - \mathrm{e}^{-\frac{E_1}{\eta_1}t}\right) & (\sigma < \sigma_s) \\ \varepsilon &= \frac{\sigma_0}{E_0} + \frac{\sigma_0}{E_1}\left(1 - \mathrm{e}^{-\frac{E_1}{\eta_1}t}\right) + \frac{\sigma_0 - \sigma_s}{\eta_2}t & (\sigma \geqslant \sigma_s) \end{aligned}\right\} \tag{1}$$

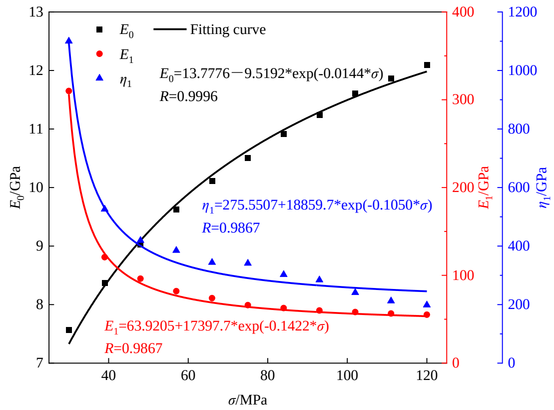


Fig. 9. Relationship between stress and $E_0$, $E_1$, $\eta_1$.

Table 2 Identification results of viscoelastic-plastic parameters.

| No. | | 30 | 39 | 48 | 57 | 66 | 75 | 84 | 93 | 102 | 111 | 120 |
|---|---|---|---|---|---|---|---|---|---|---|---|---|
| SR-30 | $E_0$ | 7.57 | 8.37 | 9.03 | 9.62 | 10.11 | 10.50 | 10.91 | 11.24 | 11.60 | 11.87 | 12.10 |
| | $E_1$ | 310 | 121 | 96 | 82 | 74 | 66 | 62 | 60 | 58 | 57 | 55 |
| | $\eta_1$ | 1100 | 427 | 419 | 385 | 344 | 341 | 323 | 310 | 299 | 292 | 286 |
| | $\eta_2$ | | | | | | | 2160 | 2160 | 1944 | 1944 | 1944 |
| SR-31 | $E_0$ | 6.44 | 7.13 | 7.73 | 8.25 | 8.72 | 9.14 | | | | | |
| | $E_1$ | 428 | 185 | 139 | 118 | 106 | 99 | | | | | |
| | $\eta_1$ | | 668 | 441 | 419 | 389 | 353 | | | | | |
| | $\eta_2$ | | | | 5567 | 5567 | 5869.5 | | | | | |
| SR-32 | $E_0$ | 5.73 | 6.39 | 6.95 | 7.45 | 7.87 | 8.21 | 8.55 | 8.80 | | | |
| | $E_1$ | 212 | 118 | 85 | 73 | 66 | 62 | 59 | 56 | | | |
| | $\eta_1$ | 484 | 302 | 250 | 219 | 197 | 187 | 178 | 174 | | | |
| | $\eta_2$ | | | | 3085 | 2880 | 2880 | 2880 | 2880 | | | |
| SR-33 | $E_0$ | 5.40 | 6.05 | 6.55 | 6.99 | 7.35 | 7.68 | | | | | |
| | $E_1$ | 238 | 112 | 82 | 70 | 63 | 59 | | | | | |
| | $\eta_1$ | 750 | 421 | 362 | 310 | 284 | 252 | | | | | |
| | $\eta_2$ | | | 2734 | 2211 | 2211 | 2211 | | | | | |
| SR-34 | $E_0$ | 5.20 | 5.82 | 6.34 | 6.93 | 7.28 | | | | | | |
| | $E_1$ | 127 | 68 | 50 | 43 | 39 | 37 | | | | | |
| | $\eta_1$ | 504 | 341 | 288 | 250 | 225 | 218 | | | | | |
| | $\eta_2$ | | | 2673 | 2673 | 2673 | 2673 | | | | | |

It can be seen from the creep curve that the viscoelastic deformation remains stable after deformation for a certain time, which is determined by viscoelastic deformation definition of the Nishihara model, and this strain increases linearly with the creep stress. The viscoelastic test results showed that $\eta_1$ and $E_1$ show the same variation trend. Therefore, it can be considered that the creep parameters $K$ ($E_0$, $E_1$, and $\eta_1$) all have a linear relationship with stress, and show a nonlinear trend under the influence of initial stress as shown in Fig. 8. The same equation (Eq. 2) is used for fitting, and the corresponding creep constants $K_c$ ($E_{c0}$, $E_{c1}$, and $\eta_{c1}$) and $\sigma_0$ ($\sigma'_0$, $\sigma''_0$, and $\sigma'''_0$) related to the initial stress can be calculated. The fitting parameters are shown in Table 3.

$$K = \frac{K_c \sigma}{(\sigma - \sigma_0)} \tag{2}$$

Table 3 Viscoelastic-plastic modulus statistics of samples with different moisture content.

| No. | $E_{c0}$/GPa | $\sigma_0$/MPa | $E_{c1}$/GPa | $\sigma'_0$/MPa | $\eta_{c1}$/GPa | $\sigma''_0$/MPa |
|---|---|---|---|---|---|---|
| SR-30 | 15.20 | 32.23 | 41.94 | 25.89 | 195.03 | 24.65 |
| SR-31 | 12.68 | 29.98 | 41.14 | 25.37 | 193.59 | 25.57 |
| SR-32 | 11.89 | 33.29 | 40.33 | 24.69 | 181.46 | 21.57 |
| SR-33 | 10.66 | 29.61 | 38.40 | 25.19 | 130.26 | 24.48 |
| SR-34 | 10.31 | 29.86 | 33.11 | 24.36 | 112.33 | 23.71 |

From the fitting results in Figure 10, it can be seen that, $E_{c0}$, $E_{c1}$, and $\eta_{c1}$ have a decreasing trend with water content, and $\sigma'_0$ and $\sigma''_0$are related to the initial stress. Therefore, in the creep process, it can be considered that for sandstone samples with different water content, viscoelastic deformation occurs only when the stress exceeds a certain creep stress level under different stresses. Moreover, the whole process of viscoelastic deformation is affected by elastic modulus ($E_{c1}$), and viscous modulus ($\eta_{c1}$). It can be seen from Table 2 that $\eta_2$ is stable at this stage with little change and is basically a constant. Therefore, plastic development is positively correlated with stress at this stage.

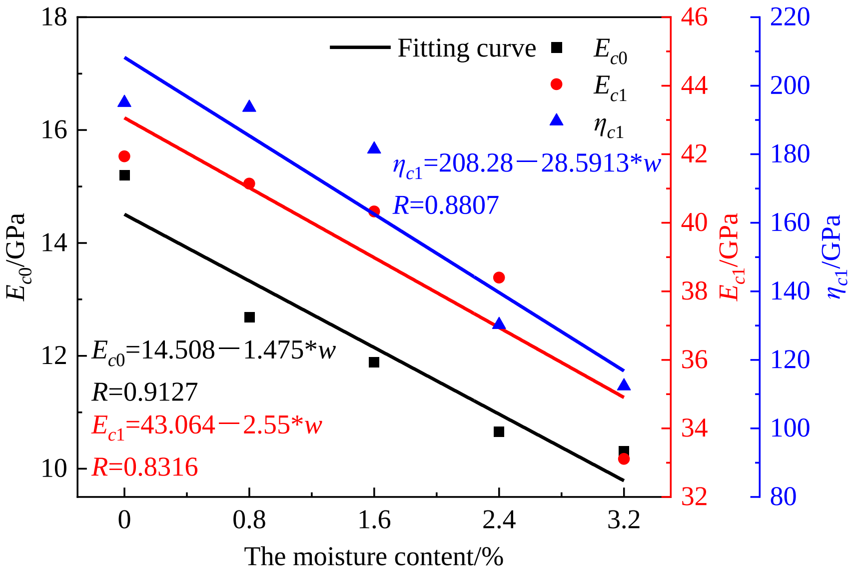


Fig. 10. Relationship between viscoelastic-plastic modulus and water content.

### 3.3 Nonlinear deformation separation

The deformation curve of nonlinear deformation stage is shown in Fig. 11. When the stress is greater than the accelerated yield limit stress, it enters nonlinear damage stage. Through isochronous curve processing, it is found that the stress level at this stage increases the damage and acts on viscoelastic and plastic deformation at the same time. A new damage model is established to describe the nonlinear deformation at this stage, as shown in Fig. 12. The model only takes effect when the stress level exceeds the accelerated yield stress. The creep expression is shown in Eq. (3), which is used to fit the creep data. In addition, sample SR-31 was not listed and calculated because it only has a first-order accelerated damage stage. The nonlinear damage parameters are shown in Table 4.

$$\varepsilon(t)=\frac{\sigma_0-\sigma_{s1}}{\eta_3}t+\frac{\sigma}{E_2}\left[1-\exp(-\frac{E_2}{\eta_4}t)\right] \tag{3}$$

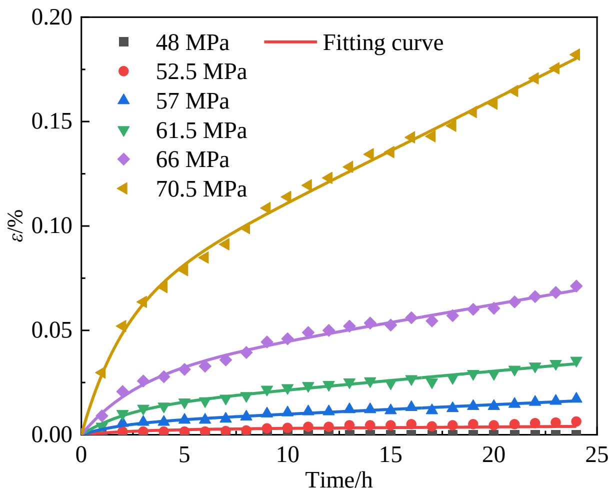


Fig. 11. Nonlinear deformation curve of sample SR-34 at the third stage.

Table 4 Fitting parameters of nonlinear damage model.

| No. | Creep stress | $\eta_3$/GPa | $E_2$/GPa | $\eta_4$/GPa |
|---|---|---|---|---|
| | 102 | 20000 | 150 | 457 |
| | 106.5 | 8000 | 95 | 350 |
| SR-30 | 111 | 4811.1 | 64.5 | 263.2 |
| | 115.5 | 3805.2 | 45.8 | 180.2 |
| | 120 | 2875.5 | 33.2 | 130.8 |
| | 66 | 230000 | 210 | 1000 |
| | 70.5 | 25394.8 | 158.7 | 714.3 |
| | 75 | 20720.1 | 130.8 | 590.5 |
| SR-31 | 79.5 | 15444.8 | 103.4 | 510.2 |
| | 84 | 11307.3 | 68.2 | 350.3 |
| | 88.5 | 6203.3 | 49.1 | 207.8 |
| | 93 | 1967.1 | 37.2 | 123.7 |
| | 57 | 6300 | 161.1 | 409 |
| | 61.5 | 1984.8 | 143 | 327.1 |
| SR-33 | 66 | 1519.3 | 75.9 | 177.1 |
| | 70.5 | 1021.8 | 48.2 | 122.8 |
| | 75 | 460.9 | 19.7 | 20.6 |
| | 52.5 | 7000 | 180 | 480.8 |
| | 57 | 1993.3 | 166.8 | 329.5 |
| SR-34 | 61.5 | 1511.8 | 106.9 | 245.6 |
| | 66 | 1057.6 | 63.4 | 173.1 |
| | 70.5 | 457.8 | 36 | 74.2 |

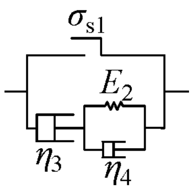


Fig. 12. Nonlinear phase damage model.

Based on the statistics and analysis of creep parameters of SR-34 in nonlinear deformation stage, it is found that $\eta_3$, $E_2$, and $\eta_4$ have nonlinear relationship with stress (Fig. 13). When the creep stress is closer to the accelerated yield limit stress, each creep parameter region is infinite and presents a power function decreasing relationship with the creep stress increasing. The fitting parameters and stress change equations are shown in Table 5.

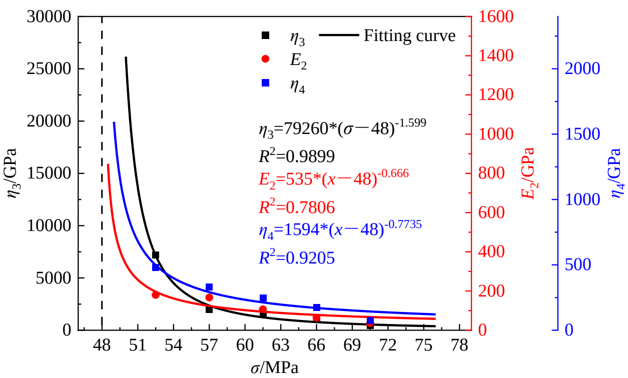


Fig. 13. Relationship between nonlinear deformation parameters and stress of SR-34.

Table 5 Nonlinear deformation fitting parameters.

| No. | Parameter | *a* | *b* | $R^2$ |
|---|---|---|---|---|
| | $\eta_3$ | $1.33\times10^5$ | -1.261 | 0.9984 |
| SR-30 | $E_2$ | 527.9 | -0.8236 | 0.9823 |
| | $\eta_4$ | 1237 | -0.6346 | 0.9292 |
| | $\eta_3$ | $1.19\times10^7$ | -2.629 | 0.9909 |
| SR-31 | $E_2$ | 603.3 | -0.6622 | 0.9047 |
| | $\eta_4$ | 2954 | -0.686 | 0.8922 |
| | $\eta_3$ | $5.64\times10^4$ | -1.461 | 0.9903 |
| SR-33 | $E_2$ | 573.5 | -0.7901 | 0.8024 |
| | $\eta_4$ | 2925 | -1.091 | 0.9406 |
| | $\eta_3$ | $7.93\times10^4$ | -1.599 | 0.9899 |
| SR-34 | $E_2$ | 535 | -0.666 | 0.7806 |
| | $\eta_4$ | 1594 | -0.7735 | 0.9205 |

In series with the Nishihara model, the creep equation can be established when the stress is greater than the accelerated yield limit damage:

$$\varepsilon(t)=\frac{\sigma_0-\sigma_{s1}}{\eta_3}t+\frac{\sigma}{E_2}\left[1-\exp(-\frac{E_2}{\eta_4}t)\right] \tag{4}$$

## 4 Accelerated creep and mathematical modelling

From the above study, the accelerated creep failure starts from a certain strain threshold and is closely related to the steady creep. Therefore, for the damage creep equation, the steady creep rate under different stress conditions can be caculated:

$$\dot{\varepsilon}(t)=\begin{cases}\dfrac{\sigma_0-\sigma_{s0}}{\eta_2}, & \sigma_{s1}>\sigma_0>\sigma_{s0}\\ \dfrac{\sigma_0-\sigma_{s0}}{\eta_2}+\dfrac{\sigma_0-\sigma_{s1}}{\eta_3}, & \sigma_c>\sigma_0>\sigma_{s1}\end{cases} \tag{5}$$

The steady-state creep rate under the corresponding creep stress can be gained from the above rules. When the creep rate reaches a certain threshold due to the increasing stress, instantaneous failure will occur. According to the traditional compression test scheme, the loading strain rate is usually $1\times10^{-4}$ (Yin et al., 2010), so it can be considered that when the strain rate is greater than this value, the rock will undergo instantaneous compression failure. The calculated ultimate creep stress under different moisture content is shown in Table 6. It can be seen that there is little difference between ultimate creep stress and compressive strength, that is, instantaneous compression failure occurs when the creep stress is large enough.

Table 6 Relationship between ultimate creep stress and compressive strength.

| Water content | Limit stress | Compressive strength | Error |
|---|---|---|---|
| 0% | 152.6 | 152 | 0.4% |
| 0.8% | 116.2 | 107.6 | 8.0% |
| 2.4% | 79.4 | 80.6 | 1.5% |
| 3.3% | 77.8 | 76.3 | 2.0% |

Based on the steady creep rate, the damage factor $D_0$ is established as the initial damage that enters into the accelerated creep to influence the accelerated creep failure (Eq. 6). Fig. 14 shows the Variation of stress damage $D_0$ with stress of SR-34.

$$D_0 = 1e4 * \dot{\varepsilon}(t) \tag{6}$$

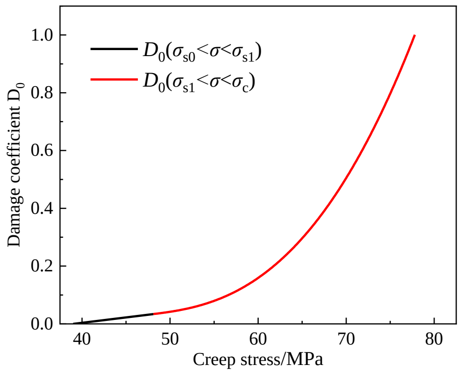


Fig. 14 Variation of stress damage $D_0$ with stress of SR-34.

Damage variable was first proposed in damage mechanics. Kachanov (1992) and Yang et al. (2014) made theoretical analysis of brittle failure of components working in high-temperature environment and proposed rock damage evolution equation based on Norton power law equation:

$$\frac{\mathrm{d}D}{\mathrm{d}t} = a\left(\frac{\sigma}{1-D}\right)^n \tag{7}$$

Where, $a$ and $n$ are material constants, $\sigma$ is tensile stress.

During the accelerated creep process, the strain rate increases gradually with time. Damage variables are introduced to describe the changes of rock microcracks in this process. In the final stage of accelerated rheology, a large number of microscopic cracks are generated and expanded in rocks, and the microscopic main cracks can gradually form and develop continuously, and finally creep failure occurs. Considering the variation of damage variables when rock reaches brittle failure, it can be considered that rock failure occurs when D=1.

The failure time can be caculated by integrating Eq. (8):

$$t_c = t_\varepsilon + \frac{(1-D_0)^{n+1}}{(n+1)a\sigma^n} \tag{8}$$

Therefore, the damage evolution equation of rock in the accelerated creep process can be provided:

$$D=1-\left[(n+1)a\sigma^{n}\left(t_{c}-t\right)\right]^{\frac{1}{n+1}}\quad\left(t_{\varepsilon}<t\leqslant t_{c}\right)\tag{9}$$

Where $t$ is time, $t_\varepsilon$ is time corresponding to accelerated creep strain, $D_0$ is the initial damage variable for the accelerated creep, $n$, $a$ is the material constant, $\sigma$ is the creep stress.

A new stress damage accelerated creep model is established according to the stress-strain relationship. When the creep strain reaches the critical threshold $\varepsilon_{s2}$, the model enters the working state. Corresponding deformation model is shown in Fig. 15, and the expression of creep parameter $\eta_5$ is shown in Eq. (10).

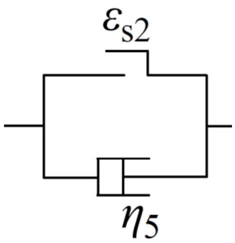


Fig. 15. Stress damage acceleration model.

$$\eta_5=\eta_5(1-D)\tag{10}$$

Thus, a complete damage creep model is established, as shown in Fig. 16. Its creep equation can be obtained according to the superposition principle, as shown in Eq. (11).

$$\varepsilon\left(t\right)=\varepsilon_{e}+\varepsilon_{ve}+\varepsilon_{vp}+\varepsilon_{vp1}+\varepsilon_{vp2}=$$

$$\begin{cases}\dfrac{\sigma_0}{E_0}+\dfrac{\sigma_0}{E_1}\left[1-\exp(-\dfrac{E_1}{\eta_1}t)\right],\sigma_0<\sigma_{s0}\\[2ex] \dfrac{\sigma_0}{E_0}+\dfrac{\sigma_0}{E_1}\left[1-\exp(\dfrac{E_1}{\eta_1}t)\right]+\dfrac{\sigma_0-\sigma_{s0}}{\eta_2}t,\sigma_{s0}\leq\sigma_0<\sigma_{s1}\\[2ex] \dfrac{\sigma_0}{E_0}+\dfrac{\sigma_0}{E_1}\left[1-\exp(-\dfrac{E_1}{\eta_1}t)\right]+\dfrac{\sigma_0-\sigma_{s0}}{\eta_2}t+\dfrac{\sigma_0-\sigma_{s1}}{\eta_3}t+\dfrac{\sigma_0-\sigma_{s1}}{E_2}\left[1-\exp(-\dfrac{E_2}{\eta_4}t)\right],\quad\sigma_0>\sigma_{s1}\\[2ex] \dfrac{\sigma_0}{E_0}+\dfrac{\sigma_0}{E_1}\left[1-\exp(-\dfrac{E_1}{\eta_1}t)\right]+\dfrac{\sigma_0-\sigma_{s0}}{\eta_2}t+\dfrac{\sigma_0-\sigma_{s1}}{\eta_3}t+\dfrac{\sigma_0-\sigma_{s1}}{E_2}\left[1-\exp(-\dfrac{E_2}{\eta_4}t)\right]\\ \qquad+\dfrac{\sigma_0-\sigma_{s1}}{\eta_5\left[(n+1)a\sigma^{n}\left(t_c-t\right)\right]^{\frac{1}{n+1}}},\quad\sigma_0>\sigma_{s1},t_\varepsilon<t\leqslant t_c\end{cases}\tag{11}$$

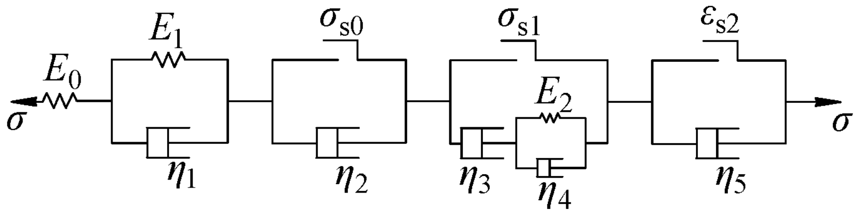


Fig. 16. Nonlinear damage creep model.

## 5. Performance of the proposed mathematical model

The model is used to fit the nonlinear rheological stress damage model and to analyze the creep experimental results of sandstone under triaxial compression. Some viscoelastic parameters can be calculated according to the parameters in Table 2 and 4, and the model parameters can be caculated according to the critical stress parameters given in Table 7. The final experimental failure curves of SR-33 and SR-34 samples were calculated by this method, as shown in Fig. 17. It can be seen that the model can better describe the initial creep and stable creep, and better express the behavior of accelerated creep failure. In addition, according to the calculation equation, the creep strain of SR-34 sample under the creep stress of 66 MPa reaches 0.434 at 86.3 h, thus entering the accelerated creep stage. Because the initial damage of the acceleration stage is small, the failure time is longer than that under the stress of 70.5MPa. The accelerated failure time was 11.2 h, and the final failure occurred at 97.5 h.

Table 7 Parameters of rock stress nonlinear damage rheological model.

| No. | Stress/MPa | $\sigma_{s0}$ /MPa | $\sigma_{s1}$ /MPa | $\eta_5$ /GPa | $n$ | $a$ | $\varepsilon$/% | $t_1$/h | $\Delta t_c$ |
|---|---|---|---|---|---|---|---|---|---|
| SR-33 | 75 | 39 | 52.5 | 113 | 1.6 | 4e-5 | 0.431 | 27.2 | 8.6 |
| SR-34 | 66 | 39 | 48 | 103 | 1.6 | 4e-5 | 0.434 | 27.5 | 9.2 |
| | 70.5 | | | | | | | 86.3 | 11.2 |

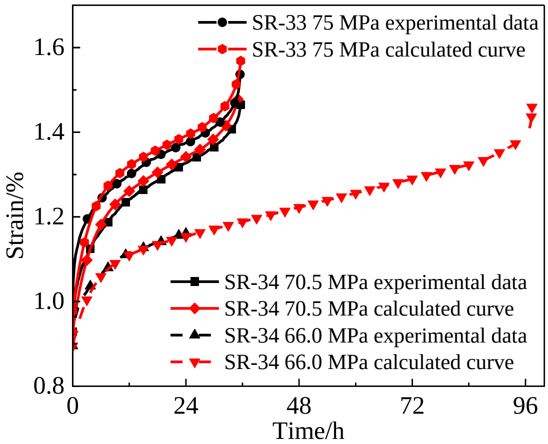


Fig. 17. Comparison between fitting curve of nonlinear damage model and experimental results.

## 6. Conclusions

1. Water has an effect on both long-term and short-term strength of sandstone, and the short-term peak strength of sandstone decreases exponentially with the increase of water content. The softening coefficient of sandstone increases from 0.372 at 0 MPa confining pressure to 0.520 at 12 MPa confining pressure, and the long-term strength also decreases with water content.
2. Based on the law of isochronous curve deformation, the creep stress can be divided into three stages. The critical stress is the yield limit (i.e. long-term strength) and the accelerated yield limit stress. The ratio of yield limit to compressive strength is between 0.48 and 0.55, and the ratio of accelerated yield limit stress to compressive strength is between 0.63 and 0.75.
3. The creep parameters $E_{c0}$, $E_{c1}$ and $\eta_{c1}$ related to the initial water content and stress were proposed, which showed a linear decreasing law with the water content. The creep model describing the nonlinear deformation is established by separating the nonlinear stage deformation. The creep parameters decrease with the stress as a power function when the accelerated yield limit stress is exceeded by the creep stress.
4. A damage factor based on steady creep rate is introduced to describe the accelerated creep behavior.

The higher the steady creep rate, the shorter the accelerated creep time. A complete creep model can be established to fit and predict creep behavior under different creep stresses, and the creep deformation law under different stress conditions can be described.

## Declaration of Competing Interest

The authors declare that they have no conflicts of interest.

## Acknowledgements

This work was supported by the National Natural Science Foundation of China (Grant No. 52174096, 52304110); the Ordos Science & Technology Plan (Grant No. TD20240003); the Ordos science and Technology Bureau (Grant No. IMRI23005); the Ordos Science & Technology Plan (Grant No.YF20240021).

## References

Aydan, M., 2017. Time-Dependency in Rock Mechanics and Rock Engineering. CRC Press.

Chen, P.Z., Tang, S.B., Liang, X., Zhang, Y.J., Tang, C.A., 2021. The influence of immersed water level on the short- and long-term mechanical behavior of sandstone. Int. J. Rock Mech. Min. Sci. 138, 104631.

Cong, L., Hu, X.L., 2017. Triaxial rheological property of sandstone under low confining pressure. Eng. Geol. 231, 45–55.

Cui, X.H., Fu, Z.L., 2006. Experimental study on rheology propertiesand long-term strength of rocks. Chin. J. Rock Mech. Eng. 25(5), 1021–1024.

Deng, H.F., Zhou, M.L., Li, J.L., Sun, X.S., Huang, Y.L., 2016. Creep degradation mechanism by water-rock interaction in the red-layer soft rock. Arab. J. Geosci. 9(12), 601.

Jiang Q, Qi Y, Wang Z, Zhou, C.Q., 2013. An extended Nishihara model for the description of three stages of sandstone creep. Geophys. J. Int. 193, 841–854.

Jiang, X.W.，Chen C.X.，Xia K.Z.，Liu, X.M., Zhou, Y.C., 2016. Experimental study of creep characteristics of gypsum mine rock in triaxial compression. Rock Soil Mech. 37(S1), 301–308.

Kachanov, M., 1992. Effective elastic properties of crack solids critical review of some basic concepts. Appl. Mech. Review. 45(7), 304–335.

Li, D., Wong, L., Liu, G., Zhang, X.P., 2012. Influence of water content and anisotropy on the strength and deformability of low porosity meta-sedimentary rocks under triaxial compression. Eng. Geol. 126, 46–66.

Lin, Q.X., Liu, Y.M., Tham, L.G., Tang, C.A., Lee, P.K.K., Wang J., 2009. Time-dependent strength degradation of granite. Int. J. Rock Mech. Min. Sci. 46(7), 1103–1114.

Liu, X., 1994. Introduction to rock rheology. Beijing：Geological Publishing House. 126–133.

Liu, X.X., Li, S.N., Zhou Y.M., Li, Y., Wang, W.W., 2020. Research on Creep Characteristics and Long-term Strength Argillaceous Siltstone Under High Stress. Chin. J. Rock Mech. Eng. 39(1), 138–146.

Lu Y.L., Wang L.G., 2017. Effect of water and temperature on short-term and creep mechanical behaviors of coal measures mudstone. Environ. Earth Sci. 76(17), 597.

Lu, Y.L., Wang, L.G., 2017. Effect of water and temperature on short-term and creep mechanical behaviors of coal measures mudstone[J]. Environ. Earth Sci. 76(17), 597.

Miao, C.Y., Yang, L., Xu, Y.Z., Yang, K., Sun, X.M., Jiang, M., Zhao, W.C., 2021. Study on strength softening experiment and micro-mechanism of sandstone based on nuclear magnetic resonance[J].

Chin. J. Rock Mech. Eng. 40(11), 2189－2198.

Özşen, H., Özkan, İ., Şensöğüt, C., 2014. Measurement and mathematical modelling of the creep behaviour of Tuzköy rock salt. Int. J. Rock Mech. Min. Sci. 66, 128–135.

Rajabzadeh, M.A., Moosavinasab, Z., Rakhshandehroo, G., 2012. Effects of rock classes and porosity on the relation between uniaxial compressive strength and some rock properties for carbonate rocks. Rock Mech. Rock Eng. 45(1):113–122.

Shan R.L., Bai Y., Sun P.F., Sui, S.M., Huang, Y.L., Chen, J.L., 2019. Study of triaxial creep mechanical properties and constitutive model of frozen stratified red sandstone. J. China Univ. Min. Technol. 48(1), 12–22.

Shan, R.L., Bai, Y., Ju, Y., Han, T.Y., Dou, H.Y., Li Z.L., 2021. Study on the Triaxial Unloading Creep Mechanical Properties and Damage Constitutive Model of Red Sandstone Containing a Single Ice-Filled Flaw. Rock Mech. Rock Eng. 54, 833–855.

Sun, X.M., Miao C.Y., Jiang M., Zhang, Y., Yang, L., Guo, B., 2021. Experimental and theoretical study on creep of sandstone with different moisture content based on modified Nishihara model. Chin. J. Rock Mech. Eng. 40(12), 2411–2420.

Tang, S.B., Yu, C.Y., Heap, M.J., Chen, P.Z., Ren, Y.G., 2018. The Influence of Water Saturation on the Short- and Long-Term Mechanical Behavior of Red Sandstone. Rock Mech. Rock Eng. 51(9), 2669–2687.

Tao, B., Wu, F.Q., Guo, G.M., Zhou, R.G., 2005. Flexibility of visco-elastoplastic model to rheological characteristics of rock and solution of rheological parameter. Chin. J. Rock Mech. Eng. 24(17), 3165–3171.

Wang, D., Chen, G.Q., Jian D.H., Zhu, J., Lin, Z.H., 2021. Shear creep behavior of red sandstone after freeze-thaw cycles considering different temperature ranges[J]. B. Eng. Geol. Environ. 80, 2349–2366.

Wang, J., Zhang, Z.J., Zhu, T.C., He, M.C., Gong, W.L., Zhang, X.Y., 2020. Model test study on deformation mechanisms of roadways supported by constant resistance and large deformation anchor cables. Chin. J. Rock Mech. Eng. 39(5), 927–937.

Wang, Y.C., Cong, L., Yin, X.M., Yang, X.Y., Zhang, B.C., Xiong, W., 2021. Creep behaviour of saturated purple mudstone under triaxial compression. Eng. Geol. 288, 106159.

Wasantha, P., Ranjith, P.G., 2014. Water-weakening behavior of Hawkesbury sandstone in brittle regime. Eng. Geol. 178, 91–101.

Wong, L., Maruvanchery, V., Liu, G., 2015. Water effects on rock strength and stiffness degradation. Acta Geotech. 11(4), 1–25.

Wu, F., Zhang, H., Zou, Q.L., Li C.B., Chen, J., Gao R.B., 2020. Viscoelastic-plastic damage creep model for salt rock based on fractional derivative theory. Mech. Mater. 150(6), 103600.

Xu, X.B., Cui, Z.D.,2020. Investigation of a fractional derivative creep model of clay and its numerical implementation. Comput. Geotech. 119, 103387.

Yan, B.Q., Guo, Q.F., Ren, F.H., Cai, M.F., 2020. Modified Nishihara model and experimental verification of deep rock mass under the water-rock interaction. Int. J. Rock Mech. Min. Sci. 128, 104250.

Yang, S.Q., Xu, P., 2014. A new nonlinear rheological damage model for rock. Chin. J. Geotech. Eng. 36(10), 1846–1854.

Yin, X.T., Ge, X.R., Li, C.G, Wang, S.L., 2010. Influences of loading rates on mechanical behaviors of rock materials. Chin. J. Rock Mech. Eng. 29(1), 2610–2615.

Yu, C., Tang, S.B., Tang, C.A., Duan, D., Zhang, Y.J., Liang, Z.Z., Ma, K., Ma, T.H., 2019. The effect of water on the creep behavior of red sandstone. Eng. Geol. 253, 64–74.

Zhang, C.H., Zhao, Q.S., 2014. Triaxial tests of effects of varied saturations on strength and modulus for sandstone. Rock Soil Mech. 35(4), 951–958

Zhang, L.L., Wang, X.J., 2020.Viscoelastic-plastic damage creep model for rock. Chin. J. Geotech. Eng. 42(6), 1085–1092.

Zheng, H., Feng, X.T., Hao, X.J., 2015. A creep model for weakly consolidated porous sandstone including volumetric creep. Int. J. Rock Mech. Min. Sci. 78, 99–107.

Zhou, H.W., Wang, C.P., Han, B.B., Duan, Z.Q., 2011. A creep constitutive model for salt rock based on fractional derivatives. Int. J. Rock Mech. Min. Sci. 48(1), 116–121.

Zhou, X.P., Pan, X.K., Cheng, H., 2021. The Nonlinear Creep Behaviors of Sandstone Under the Different Confining Pressures Based on NMR Technology. Rock Mech. Rock Eng. 54, 4889–4904.